nature communications

Article

https://doi.org/10.1038/s41467-025-61301-3

Noninvasive cardiac modulation via triplet-sensitized photoswitching in the phototherapeutic window

Received: 8 July 2024

Accepted: 18 June 2025

Published online: 10 July 2025

Check for updates

Lukas Naimovičius[1,2], Mila Miroshnichenko[1], Ekin Opar[3,4,5], Helen Hölzel[6], Masa-aki Morikawa[7], Nobuo Kimizuka[7], Manvydas Dapkevičius[2], Justas Lekavičius[2], Edvinas Radiunas[2], Karolis Kazlauskas[2], Víctor Cilleros-Mañé[3,4], Fabio Riefolo[3,4], Carlo Matera[3,4,8], Kevser Harmandar[9], Masahiko Taniguchi[10], Fabienne Dumoulin[9], Jonathan S. Lindsey[10], Pankaj Bharmoria[1] ✉, Pau Gorostiza[3,4,11] ✉ & Kasper Moth-Poulsen[1,6,11,12] ✉

Red, far red, or near-infrared photoswitchable drugs offer immense photopharmacological advantages due to the higher light penetration through the skin. Such photoactivation is achieved using processes such as two- and three-photon absorption, excited-state absorption, and triplet-triplet annihilation upconversion, which require higher photon fluences (W to kW cm^{-2}) than the resilience constraints of skin (200 mW cm^{-2}). Herein, a generalized approach of *cis*-to-*trans* photoisomerization of azobenzenes is demonstrated via triplet sensitization with NIR-I illumination (850 nm) of a new Zn-octa-substituted phthalocyanine photosensitizer, in aqueous medium at 2.62 mW cm^{-2}. The approach is applied to control the heart rate of a frog tadpole via *cis*-to-*trans* photoisomerization of an azobenzene-functionalized muscarinic acetylcholine receptor M_2 agonist in the phototherapeutic window (730 nm excitation: 42 mW cm^{-2}). This advance highlights a powerful photo-pharmacological strategy for modulation of in vivo activity at 2-4 orders of magnitude lower photon fluences of NIR light compared to established methods.

Biological photoactivation upon far-red (FAR) and near infra-red (NIR) light excitation enables numerous in vivo applications such as bioimaging[1], biosensing[2], drug delivery[3,4], optogenetic neural modulation[5,6], cardiac defibrillation[6,7], and photodynamic therapy[8,9]. This is due to the higher penetration of FAR/NIR light through living tissue in the phototherapeutic window (Fig. 1a and Supplementary Fig. 9)[10]. A very attractive phenomenon for photochemical control is a change in molecular shape. In this regard, the photoinduced geometrical interconversion of *cis-trans* isomers can enable control of biological activity when functionalized with a suitable drug molecule[11].

[1]Institute of Materials Science of Barcelona, ICMAB-CSIC, Bellaterra, Barcelona, Spain. [2]Institute of Photonics and Nanotechnology, Vilnius University, Vilnius, Lithuania. [3]Institute for Bioengineering of Catalonia (IBEC), The Barcelona Institute of Science and Technology, Barcelona, Spain. [4]CIBER-bbn (biomaterials, bioengineering, and nanomedicine), Barcelona, Spain. [5]Doctorate Program in Engineering and Applied Science, University of Barcelona, Barcelona, Spain. [6]Department of Chemical Engineering, Universitat Politècnica de Catalunya, EEBE, Eduard Maristany 10–14, Barcelona, Spain. [7]Department of Applied Chemistry, Graduate School of Engineering, Center for Molecular Systems (CMS), Kyushu University, Fukuoka, Japan. [8]Department of Pharmaceutical Sciences, University of Milan, Milan, Italy. [9]Acıbadem Mehmet Ali Aydınlar University, Faculty of Engineering and Natural Sciences, Biomedical Engineering Department, Ataşehir, Istanbul, Türkiye. [10]Department of Chemistry, North Carolina State University, Raleigh, NC, USA. [11]Catalan Institution for Research & Advanced Studies, ICREA, Pg. Lluís Companys 23, Barcelona, Spain. [12]Department of Chemistry and Chemical Engineering, Chalmers University of Technology, Kemivagen 4, Gothenburg, Sweden. ✉e-mail: pbharmoria@icmab.es; pau@icrea.cat; kasper.moth-poulsen@upc.edu

https://doi.org/10.1038/s41467-025-61301-3

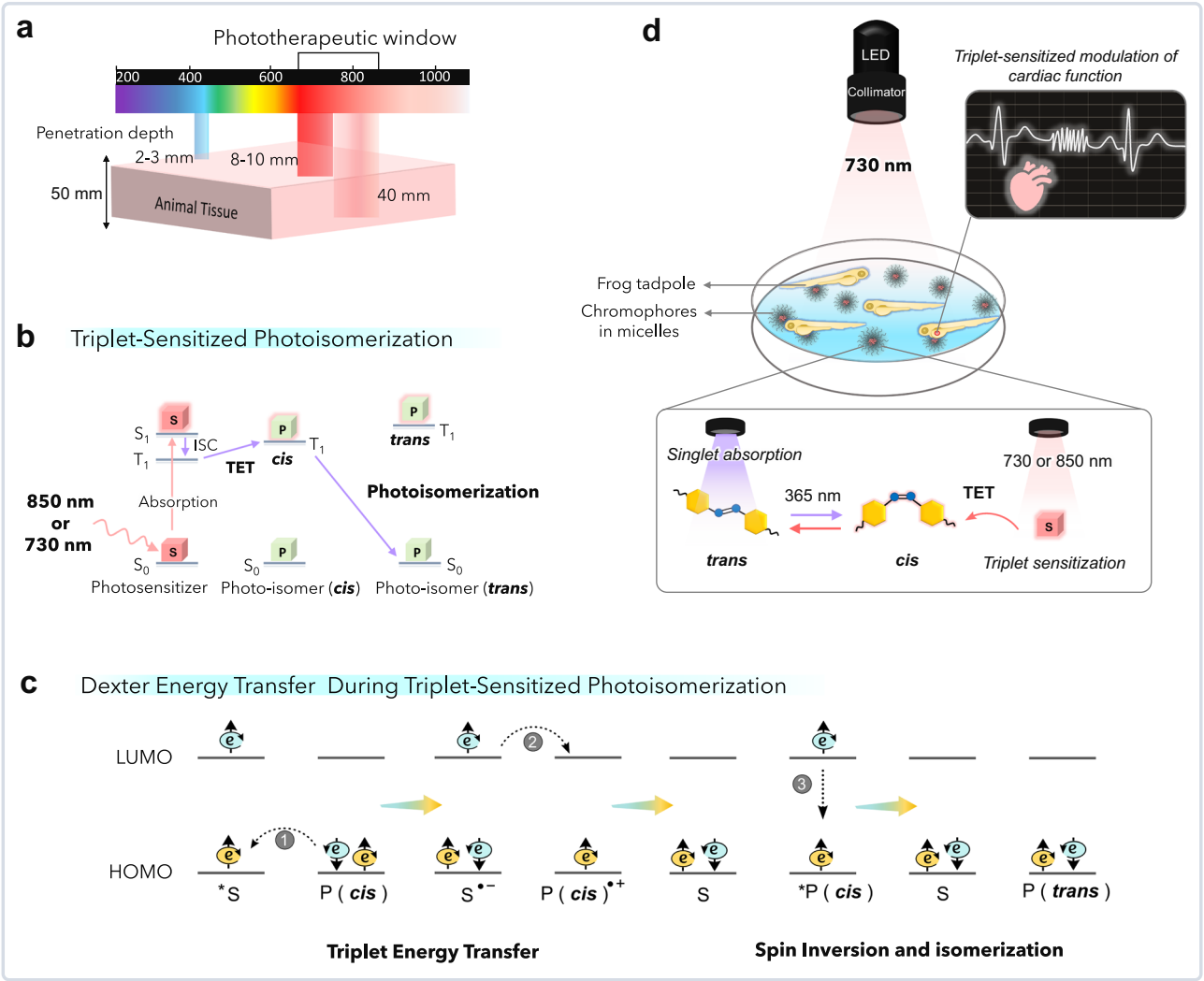

Fig. 1 | Illustration of noninvasive cardiac modulation via triplet-sensitized photoswitching in the phototherapeutic window. a Penetration depth of various wavelengths of solar energy in animal tissue. **b** Energy diagram of the low-energy excitation-based triplet-sensitized photoswitching. **c** Electron exchange via Dexter energy transfer due to the endothermic triplet energy gap between photosensitizer and photoisomer. **d** Triplet-sensitized photoswitching of azobenzene in aqueous solution after excitation-based 730 or 850 nm LED and modulation of the cardiac functions of the frog tadpole. S = photosensitizer, P = photoisomer, *e* = electron.

Photoisomerization offers several benefits compared to traditional photolysis techniques for in vivo photoactivation, as chemical by-products are not produced within the cell[12]. As a result, several photoswitches (azobenzene, thioindigo, hydrazone, diarylethene, spiropyran, donor-acceptor Stenhouse adducts[13], and norbornadiene) have been tested for biological photoactivation employing linear[14] or non-linear optical processes[15–17]. Azobenzenes have become widely recognized among the various photoswitches available. This is primarily due to their small size and molecular design flexibility, remarkable resistance to photobleaching and rapid photoisomerization, making them highly sought-after in the realm of biological activity. Consequently, these compounds have been extensively investigated in numerous research studies[18–22]. The *trans*-azobenzene is 10–12 kcal mol^{-1} more stable than the *cis*-azobenzene in the dark, hence the unsubstituted *cis* isomer eventually converts to the *trans* isomer via thermal relaxation in a few days. However, isomerization rates can be increased up to seconds via illumination at appropriate wavelengths. The *trans*-azobenzene (*E*) shows strong π-π* absorption at 320 nm and weak n-π* absorption at 440 nm. The *cis*-azobenzene (*Z*) shows n-π* absorption at 440 nm along with the π-π* absorptions at 280 and 250 nm[23]. Despite the desired photochemical stability of azobenzene, the low penetration depth of its absorption wavelengths is incompatible with in vivo applications. This issue has been addressed by red-shifting the photoswitching wavelengths with different strategies, including (i) chemical engineering of absorption wavelengths[24,25] and (ii) indirect excitation with upconverted ultraviolet-blue photons via non-linear optical processes like two-and 3 photon absorption (2-3PA) or triplet-triplet annihilation (TTA)[26–31]. Both multiphoton absorption[32,33] and excited state absorption/energy transfer upconversion (ESA/ETU)[34,35] necessitate a high photon fluence (W cm^{-2} to kW cm^{-2}) to achieve the simultaneous absorption of two or three coherent photons or excitation of a higher energy state (Supplementary Fig. 10a, b)[36]. On the contrary, TTA-UC involves a multi-component and multistep energy-transfer process that also demands high photon fluence for NIR-to-visible photon upconversion (Supplementary Fig. 10c)[5,37]. Hence, a feasible resolution lies in the utilization of an alternative photophysical mechanism that functions effectively under low photon fluences within the phototherapeutic window[38]. In the present study, triplet-sensitized photoisomerization (Fig. 1b, c) is explored for achieving biological photoactivation at low-energy excitation levels (λ_{ex} = 730 or 850 nm).

The triplet-sensitized photoisomerization enables the action spectrum of azobenzenes to be shifted into the therapeutic window (730–850 nm), with photon fluence ranging between 2-4 orders of

https://doi.org/10.1038/s41467-025-61301-3

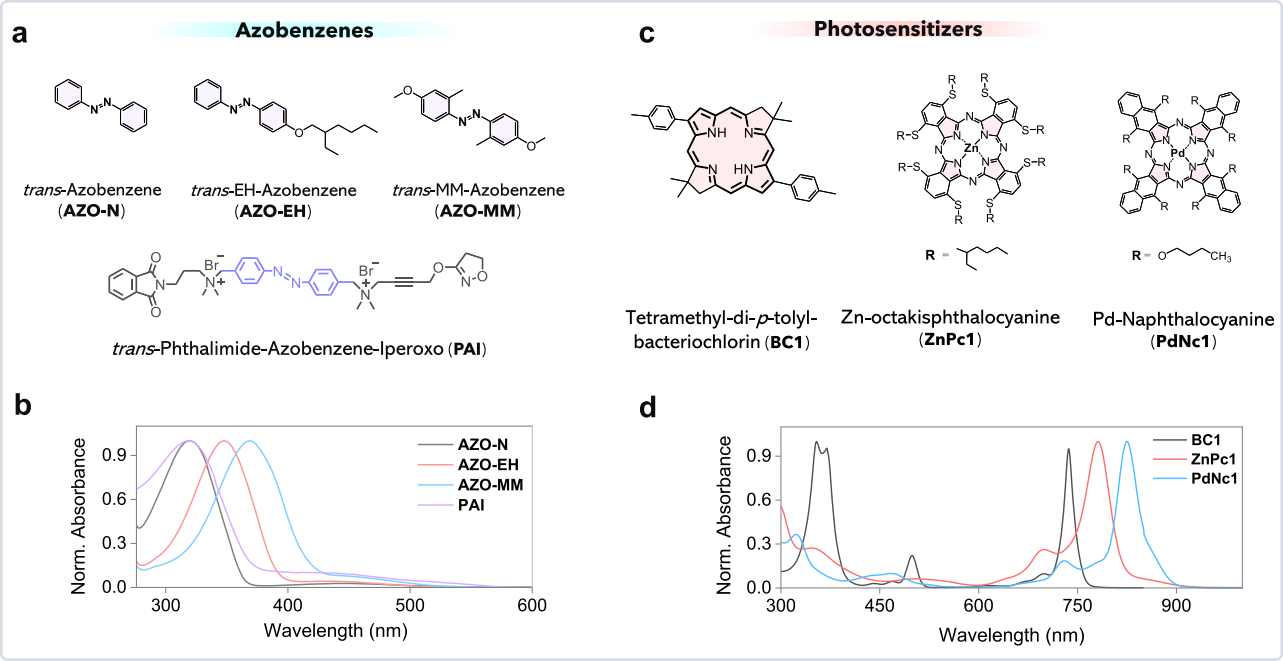

Fig. 2 | Molecular structures and absorption spectra of chromophores. Molecular structures of (**a**) azobenzenes (**AZO-N, AZO-EH, AZO-MM** and **PAI**) and (**c**) triplet photosensitizers (**BC1, ZnPc1** and **PdNc1**). Normalized absorption spectra of (**b**) azobenzenes (Conc. = 40 μM) and (**d**) triplet photosensitizers (Conc. = 4 μM) dissolved in toluene. The absorption spectrum of **PAI** was recorded in phosphate buffer solution, pH 7.4 (Conc. = 10 μM).

magnitude lower compared to 2PA, 3PA, ESA, ETU, and TTA techniques[32–37], as required for biological photoactivation (Fig. 1d). The strategy is extended to the in vivo photoisomerization of an azobenzene-modified muscarinic acetylcholine receptor M_2 agonist[15], which enabled regulation of the heart rate of a frog tadpole (Fig. 1d). While azobenzene-functionalized drugs have been increasingly utilized to selectively modulate cellular functions in vivo[15–22,31], the present study showcases the pharmacological potential of triplet sensitization via low-intensity FAR or NIR light in a real-world biomedical application. Sensitized photoisomerization of various photoswitches (azobenzene, spiropyran, diarylethene, norbornadiene, and stilbene) via triplet manifolds has been known since the 1960s. However, most of these studies were carried out upon excitation with a pulsed laser in the UV-Vis region for mechanistic understanding (see Supplementary Table 1 refs. S15–S23). Studies on triplet-sensitized photoisomerization with FAR light have recently gained momentum, especially with azobenzenes[39–41] and diazocines[42]. The lowest n-π* triplet energies of unsubstituted *cis* and *trans* azobenzene are reported at 1.26 eV and 1.53 eV, respectively[43]. Due to the energetic proximity of the triplets and the *cis-trans* photo-stationary state, and the preference of the triplet-state to relax to the *trans* form, it is possible to photoisomerize mainly the *cis* isomer to the *trans* isomer via triplet sensitization[44], barring exceptional cases of disequilibration of azobenzene by sensitization under confinement[39]. Recently, the groups of Durandin[40] and Moth-Poulsen[41] reported proof-of-concept red/far-red triplet-sensitized *cis*-to-*trans* photoisomerization of azobenzene derivatives in de-aerated organic solvents and bioplastics, respectively[40,41]. However, further shifting the action spectrum into the NIR for deep tissue photoactivation[45] is only one of a handful of design criteria that must be satisfied, together with the following: (1) the photoisomerization must operate in bio/biomimetic environments; (2) the photosensitizer and photoswitch must have suitable triplet energies for effective energy transfer; (3) the photosensitizer must be biocompatible; and (4) oxygen quenching of the chromophore triplet states must be limited. This study involves a comprehensive experimental investigation aimed at addressing the aforementioned criteria.

Results

Strategy of triplet sensitized photo-isomerization of azobenzenes

A systematic triplet-sensitized photoisomerization study has been carried out in biomimetic systems to investigate azobenzene photoswitches, and biocompatible FAR or NIR-absorbing triplet photosensitizers (Fig. 2) suitable for use in animal tissue.

First, given that animal skin is mainly comprised of collagen and lipids[46], a biomimetic surrogate for animal skin has been constituted that is composed of collagen doped with a liquid surfactant forming a micellar membrane and containing photosensitizers and azobenzenes. Second, the skin biomimetic films were placed under an 8 mm thick dried Iberian ham layer to observe photoswitching with light that can penetrate animal tissue. Each azobenzene was examined for *cis*-to-*trans* photoswitching upon excitation with 730 or 850 nm LED light through triplet sensitization in the air at very low photon fluences. Third, further photoswitching experiments were carried out with the azobenzene-containing *trans*-Phthalimide-Azobenzene-Iperoxo (**PAI**) drug encapsulated in Pluronic F-127 (PF-127) micelles in combination with the triplet photosensitizer Zn phthalocyanine (**ZnPc1**) in a phosphate buffer solution at physiological pH to mimic the cellular environment. Fourth, the **ZnPc1-PAI** system, which exhibited *cis*-to-*trans* photoswitching upon 730 nm LED excitation in air, was utilized for an in vivo experiment involving frog tadpoles to regulate cardiac rate. Each of these is now described in depth.

Azobenzenes and triplet photosensitizers

Four azobenzene compounds with distinct structural features (Fig. 2a) and absorption maxima (Fig. 2b) were chosen to understand the suitable molecular design for application in a biological setting. The parent azobenzene (**AZO-N**) was derivatized to increase the conformational flexibility for fast isomerization in restricted matrices such as films[47]. Derivatization also shifted the absorption energies. Compared to the native *trans*-azobenzene **AZO-N** (λ_{abs} = 320, 445 nm), **AZO-EH** and **AZO-MM** exhibit the π-π* absorption band red-shifted by 28 and 48 nm, respectively, whereas the n-π* band is blue-shifted by

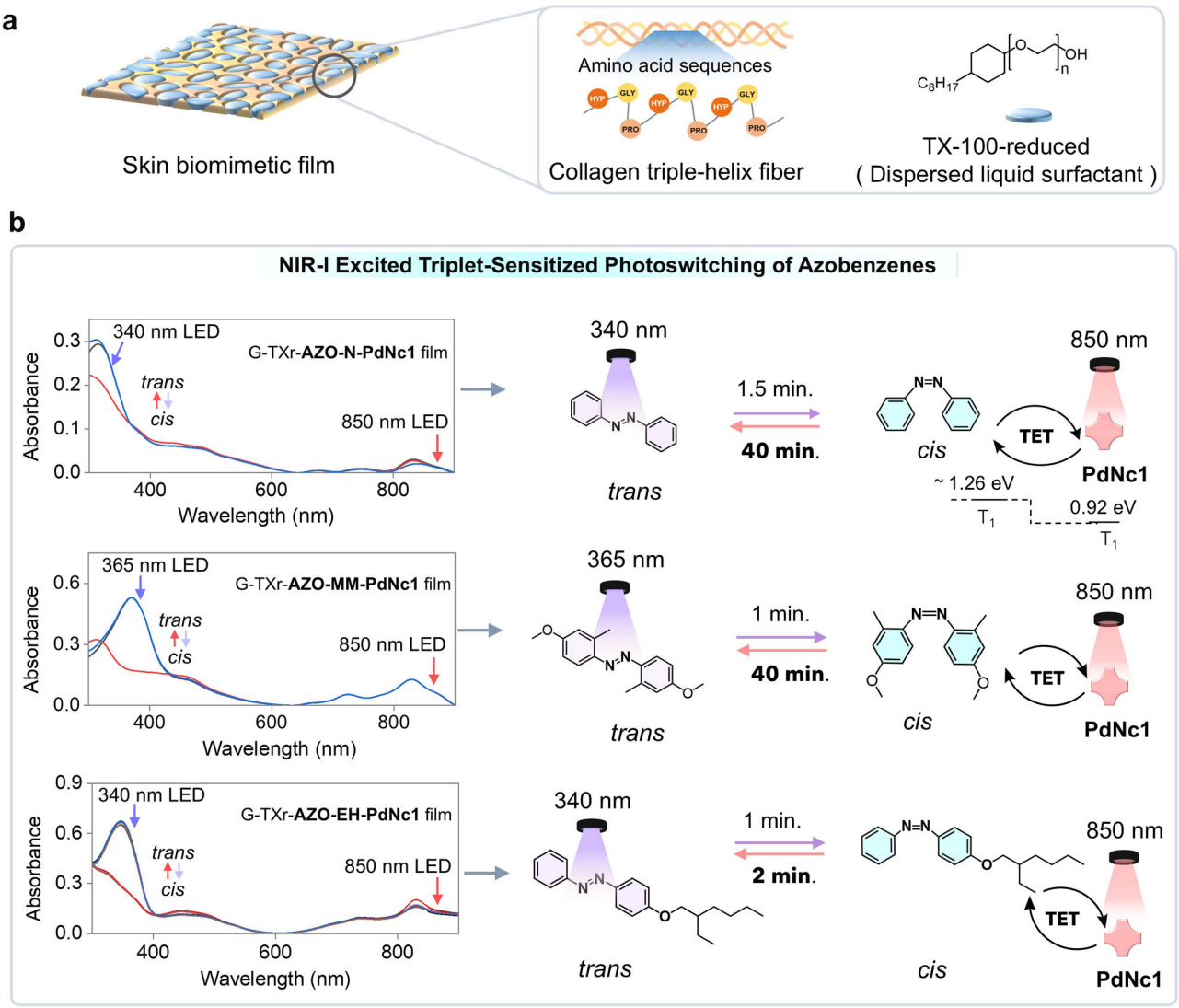

Fig. 3 | NIR-I excited triplet-sensitized photoisomerization of azobenzene. **a** Schematic illustration of the biomimetic film. **b** Absorption profiles and illustrations of forward (*trans*-to-*cis*) and backward (*cis*-to-*trans*) photoisomerization of azobenzenes in the **G-TXr-AZO-PdNc1** films via singlet absorption (λ_{ex} = 340 or 365 nm, I_o = 2.85 mW cm^{-2}) and triplet sensitization (λ_{ex} = 850 nm, I_o = 107 mW cm^{-2}), respectively.

9 nm (**AZO-EH**) or red-shifted by 15 nm (**AZO-MM**) (Fig. 2a, b). The synthesis procedure of the newly designed **AZO-MM** is provided in the experimental section of the Supplementary Information.

Three macrocycles were examined as photosensitizers (Fig. 2c), each of which absorbs strongly in the FAR or NIR region (Fig. 2d). Bacteriochlorin **BC1** is a metal-free analog of Nature's NIR absorber bacteriochlorophyll *a*[48,49]. **BC1** shows a Q_y band (S_0 - S_1, ε_{737nm} = 8.6 × 10^4 M^{-1} cm^{-1}) in the FAR region, the Q_x band (S_0-S_2) in the blue-green region (499 nm), and nominal B_x (S_0-S_3) and B_y (S_0 - S_4) bands in the blue-violet (Soret) region at 370 and 354 nm, respectively[50]. A high quantum yield of intersystem crossing (Φ_{ISC} = 0.53)[51] characteristic of bacteriochlorophylls makes such macrocycles potent triplet populators[51]. However, the short triplet lifetime makes it difficult to measure its phosphorescence at room temperature. Indeed, the phosphorescence spectrum of **BC1** in a polystyrene matrix at 10 K could not be detected (Supplementary Fig. 11). Therefore, in this study, the triplet energy (T_1 = 1.17 eV)[51] has been considered as the approximate value for **BC1**.

For NIR sensitization in vivo, a new phthalocyanine photosensitizer, 1,4,8,11,15,18,22,25-octakis(2-ethylhexylsulfanyl) Zn(II) phthalocyanine (**ZnPc1**), which bears eight alkylthio substituents in non-peripheral positions, has been designed and synthesized to display a bathochromically shifted absorption maximum (see the experimental section of the Supporting Information). **ZnPc1** exhibits a Q-band absorption maximum at 781 nm (ε_{781nm} = 2.2 × 10^5 M^{-1} cm^{-1})[52] with a tail extending to 900 nm (Fig. 2c, d). Attempts to measure its phosphorescence in a polystyrene matrix at 40 K did not yield a detectable spectrum (Supplementary Fig. 12). Owing to its structural similarity with a previously reported FAR-absorbing Zn phthalocyanine, the same triplet energy (T_1 = 1.12 eV)[41] has been employed in this study. Because the exact triplet energies of **BC1** and **ZnPc1** could not be determined, palladium naphthalocyanine **PdNc1** (Fig. 2c, d), having Q-band absorption at 825 nm (ε_{825nm} = 9.4 × 10^5 M^{-1} cm^{-1}) and triplet state at 0.92 eV (Supplementary Fig. 13), has been used for proof-of-concept NIR sensitization studies in the skin biomimetic films.

Photoisomerization studies in the skin biomimetic film

Films were prepared by combining **PdNc1** with the three azobenzene compounds dispersed in the interstitial liquid surfactant phase surrounded by collagen fibers (Fig. 3a)[41]. Hydrolyzed collagen, known as gelatin (**G**), has high solubility in water yet undergoes cross-linking upon dehydration to form a collagen-like triple-helix with a thick

https://doi.org/10.1038/s41467-025-61301-3

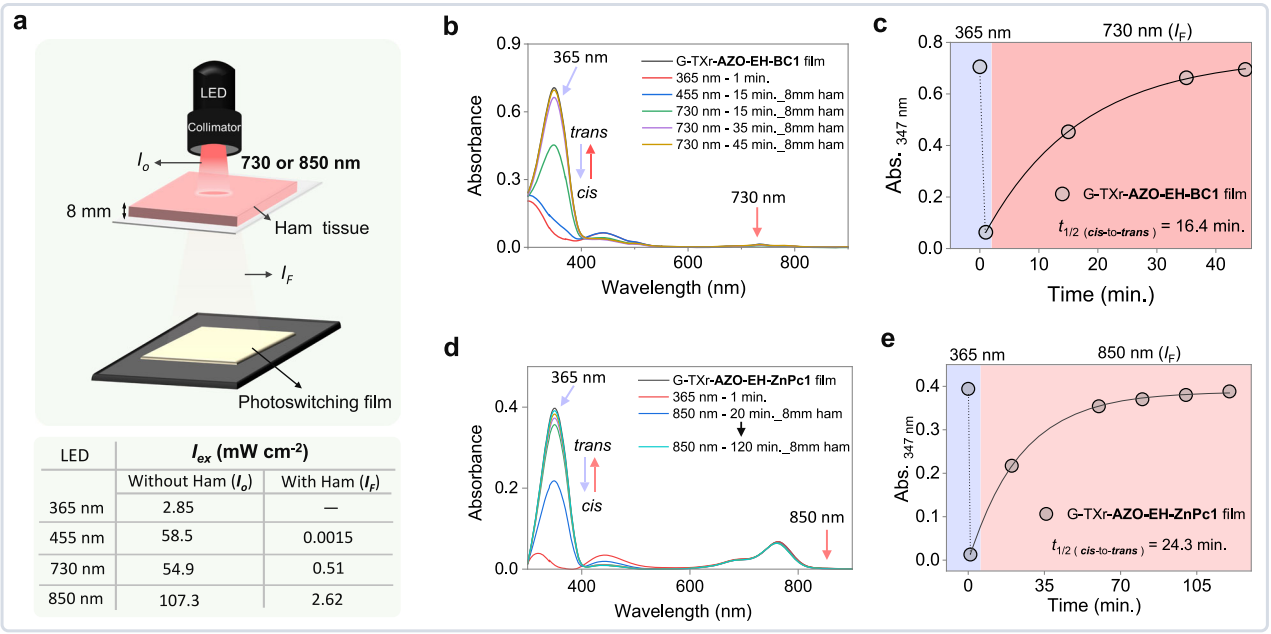

LED	I_{ex} (mW cm^{-2})	
	Without Ham (I_o)	With Ham (I_F)
365 nm	2.85	—
455 nm	58.5	0.0015
730 nm	54.9	0.51
850 nm	107.3	2.62

Fig. 4 | Triplet-sensitized photoisomerization of azobenzene in biomimetic film with a ham layer. a Schematic of the excitation with different LEDs of the biomimetic film placed below the 8 mm ham layer. The table shows the excitation intensities of different LEDs used in mW cm^{-2}. **b**, **c** Absorption profile, and kinetics of *cis*-to-*trans* photoisomerization of the G-TXr-**AZO-EH-BC1** film with ham-penetrated 730 nm LED excitation (I_F = 0.51 mW cm^{-2}). **d**, **e** Absorption profile, and kinetics of *cis*-to-*trans* photoisomerization of **G-TXr-AZO-EH-ZnPc1** film with dried Iberian ham-penetrated 850 nm LED excitation (I_F = 2.62 mW cm^{-2}).

fibrous structure that acts as an oxygen barrier[53]. As a liquid surfactant, Triton-X-100 reduced (**TXr**) was utilized due to its globally accepted low toxicity (compared to Triton-X-100)[54] and its ability to emulsify gelatin effectively[41,55]. The preparation of the films is described in the experimental section (see the Supplementary Information). The final concentrations of azobenzenes and **PdNc1** in the films were 1.95 mmol kg^{-1} and 204 μmol kg^{-1}, respectively, to keep the absorbance below 1.0. Upon dehydration, the expected triple-helix semi-crystalline structure of gelatin is retained in the **G-TXr-AZO-PdNc1** films (P-XRD Supplementary Fig. 14a, b)[41,56]. Cross-section SEM images showed interstitial TXr-chromophores in the liquid dispersed between the fibrous structure of gelatin in the **G-TXr-AZO-EH** film (Supplementary Fig. 15)[41]. Compared to toluene, in the films the π-π* band underwent a 6 nm blue-shift (**AZO-N**) or a 2 nm red-shift (**AZO-MM**), which is indicative of aggregation (Supplementary Fig. 16a, b). By contrast, no shift was observed for **AZO-EH** in the **G-TXr-AZO-EH** film, consistent with molecular dispersion (Supplementary Fig. 16c).

The photoisomerization of the azobenzenes in the **G-TXr-AZO-PdNc1** films in the air is shown in Fig. 3b. All films showed *trans*-to-*cis* photoisomerization upon LED excitation for 1 min at their normal absorption wavelengths (340 and 365 nm). In contrast, *cis*-to-*trans* photoisomerization occurred upon 850 nm excitation via triplet sensitization with **PdNc1**, thus shifting the action spectrum of the azobenzenes from 455 nm to 850 nm. The *cis*-to-*trans* photoisomerization of azobenzene at 850 nm surpasses the previous limits of 770 nm in solution[40] and of 740 nm in the solid-state[41]. Interestingly, triplet sensitization occurred despite the low triplet energy of **PdNc1** compared to that of *cis*-azobenzene compounds[57–60]. Hence, the electron exchange occurs via a Dexter energy-transfer mechanism (Fig. 1c)[57,58]. The involvement of triplet sensitization as the major driving force for *cis*-to-*trans* photoisomerization was confirmed by a control experiment in air-saturated **AZO-EH-PdNc1** toluene solution, whereupon excitation at 850 nm elicited no photoisomerization. The kinetics of *cis*-to-*trans* photoisomerization were the fastest (2 min) in the **G-TXr-AZO-EH-PdNc1** film. Therefore, **AZO-EH** was chosen for further studies with other photosensitizers in the film and in micellar solution.

The fast kinetics can be attributed to the higher conformational flexibility of **AZO-EH** in the condensed phase due to its liquid nature versus that of **AZO-N** and **AZO-MM**, which are solids at room temperature. The durability of photoisomerization in the **G-TXr-AZO-EH-PdNc1** film was confirmed by measuring the photoisomerization for 13 consecutive cycles (Supplementary Fig. 17). The possible bio-incompatibility of **PdNc1** due to the heavy metal prompted examination of **BC1** and **ZnPc1** for 730 nm and 850 nm sensitization (Fig. 2c, d) to cover the broad FAR and NIR absorption range in the phototherapeutic window. Both **G-TXr-AZO-EH-BC1** and **G-TXr-AZO-EH-ZnPc1** films showed efficient triplet-sensitized *cis*-to-*trans* photoisomerization in the films (10 s or 10 min) upon 730 nm (I_o = 54.9 mW cm^{-2}) or 850 nm (I_o = 107 mW cm^{-2}) LED excitations (Supplementary Fig. 18). The photoisomerization was faster upon excitation at 730 nm, consistent with a lesser energy difference between the triplet states of **BC1** and **AZO-EH** versus those of **ZnPc1** and **AZO-EH**. The slower observed photoisomerization process in **ZnPc1** compared to **PdNc1** can be attributed to the low extinction coefficient of **ZnPc1** at 850 nm. The involvement of the triplet state in energy transfer was confirmed by experiments in **AZO-EH-ZnPc1**-toluene solution in the absence or presence of air, where photoisomerization was observed only in the de-aerated solution (Supplementary Fig. 19).

To conduct deep tissue biomimetic experiments, an initial assessment of the viability of photoisomerization was done by positioning films of **G-TXr-AZO-EH-BC1** and **G-TXr-AZO-EH-ZnPc1** beneath an 8 mm thick layer of dried Iberian ham (Supplementary Fig. 20), followed by excitation at 730 or 850 nm (Fig. 4a).

The real-time configuration can be observed in Supplementary Fig. 21. Excitation at 365 nm of both films was performed without the ham layer due to the absorption of various bio-absorbents in the ham layer at this wavelength (as shown in Supplementary Fig. 9). The table in Fig. 4a displays the recorded values of excitation power densities (I_{ex}) of different LEDs without (I_o) and with the ham layer (I_F) utilized for the photoisomerization experiments. Indeed, only 0.0025% of 455 nm, 1% of 730 nm, and 2.44% of 850 nm light penetrated through

https://doi.org/10.1038/s41467-025-61301-3

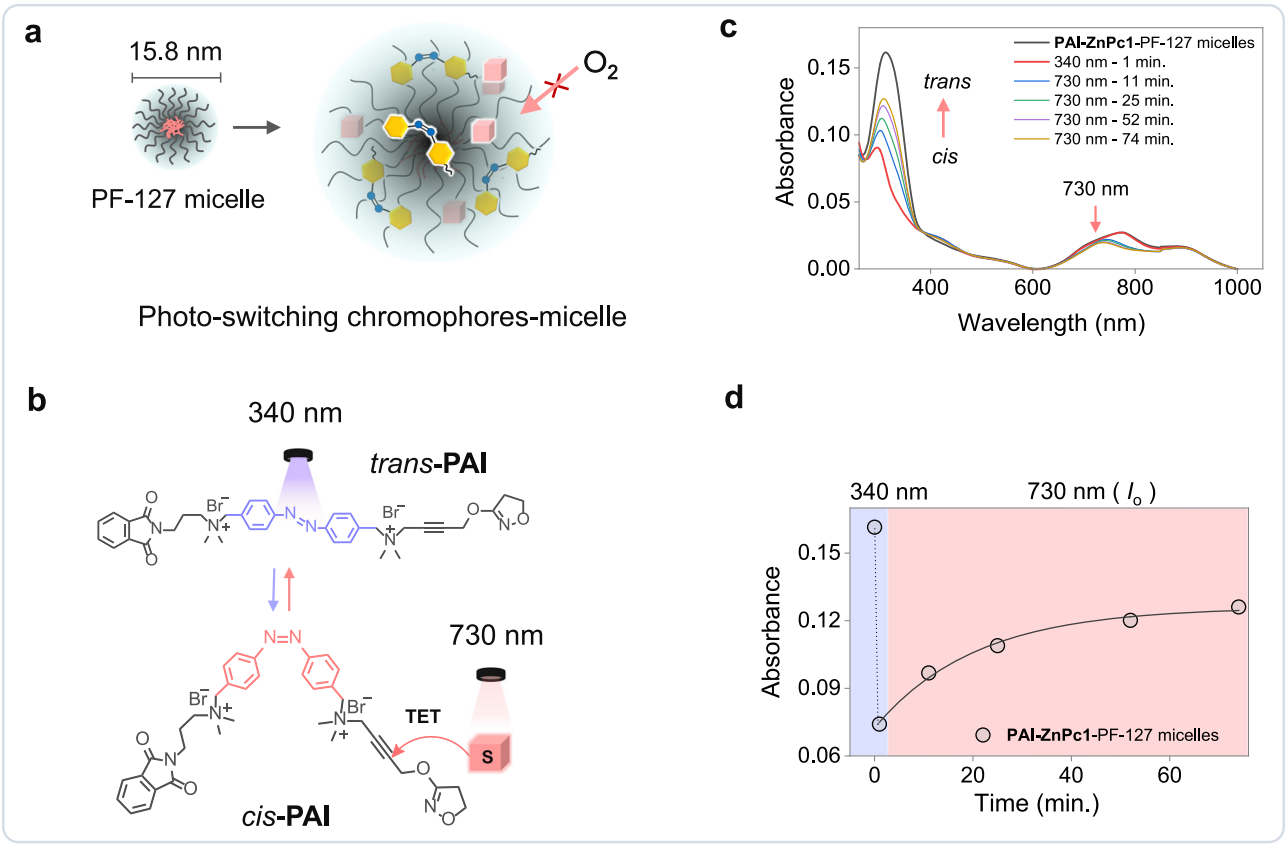

Fig. 5 | Triplet sensitized photoisomerization of azo-drug in PF-127 micelles. **a** Illustration of chromophores in PF-127 micelles in phosphate buffer pH 7.4 (25 mM). **b** Illustration of *trans*↔*cis* photoisomerization of **PAI** upon 340 and 730 nm LED excitations. **c**, **d** Absorption spectra, and kinetics of *cis*-to-*trans* photoisomerization of **PAI** in PF-127-**PAI-ZnPc1** micelles solution upon 730 nm LED excitation (I_o = 46 mW cm^{-2}). **PAI** = 50 μM, **ZnPc1** = 3 μM and PF-127 = 2%. The spectra were recorded in a 0.1 cm pathlength quartz cuvette.

the 8 mm ham layer. Prior to the photoisomerization experiments with I_F, the intensity dependence of the *cis*-to-*trans* photoisomerization was examined for the **G-TXr-AZO-EH-ZnPc1** film under 850 nm LED excitation (I_o) for 10 min. A non-linear relationship between the excitation intensity and the NIR triplet-sensitized *cis*-to-*trans* isomerization of **AZO-EH** was observed (as depicted in Supplementary Fig. 22).

Subsequent *cis*-to-*trans* photoisomerization experiments were conducted in the films using LEDs at different I_F (Fig. 4a–e). The penetration through the skin of different wavelengths is illustrated in Fig. 4b, where faster photoisomerization was observed upon a 15-min exposure with I_F excitation of 730 nm versus the actual absorption wavelength of the azobenzene at 455 nm. The slow *cis*-to-*trans* isomerization ($t_{1/2}$ = 16.4 min) was observed due to the low fluence of 730 nm irradiation (I_F = 0.51 mW cm^{-2}) as shown in Fig. 4c, consistent with the intensity dependence of isomerization (Supplementary Fig. 22) but perhaps altered in part by scattering of the incident light. A further shift in the action spectrum in the NIR-I region (850 nm) in the **G-TXr-AZO-EH-ZnPc1** film was achieved, as indicated by *cis*-to-*trans* photoisomerization even at the low photon fluence of 2.62 mW cm^{-2} (Fig. 4d). The isomerization was slow ($t_{1/2}$ = 24.3 min) due to the low fluence, low absorption coefficient of **ZnPc1** at 850 nm, and the higher endothermic triplet energy gap between the *cis*-**AZO-EH** and **ZnPc1** triplets. However, photoactivation via triplet sensitization is still possible at such low fluences after passing through the ham layer. The fluence for FAR/NIR triplet-sensitized photoactivation is between 2-4 orders of magnitude lower compared to 2-3PA, ESA, and TTA-based in vivo photoactivation applications[32–37]. Additionally, the maximum I_o used here (54 or 107 mW cm^{-2}) is well below the maximum tolerance limit of the human skin in these regions (200 mW cm^{-2})[61]. The past decade has witnessed remarkable advances in drugs containing azobenzene photoswitches for selective photoactivation in delivery, signaling, and channel activation[15–22]. The triplet-sensitized photoisomerization of azobenzenes within the phototherapeutic range and with fluences compatible with human skin constitutes an alternative strategy of remarkable potential for use in living organisms. To conduct real-time biological experiments, however, the photosensitizer-photoswitch pair must be delivered to the cell in an active state. Hence, to assess the viability of this method in a comparable setting, further experiments were conducted in aqueous micelles, as described in the next section.

Photoisomerization studies in PF-127 micelles

To explore conditions suitable for applications in biological systems, triplet-sensitized photoisomerization experiments were conducted in a phosphate buffer solution (25 mM, pH 7.4) with PF-127 micelles (2%) at room temperature. Concentrations of the photosensitizer (0.8 μM) and **AZO-EH** (24 μM) were comparable to those employed in photopharmacology. PF-127 (Fig. 5a and Supplementary Fig. 23) micelles are attractive due to their oxygen barrier capabilities[5] and biocompatibility[62]. The experimental setup, featuring an 8 mm ham layer, is illustrated in Supplementary Fig. 24. In the micellar solution, **AZO-EH** exhibited typical *trans*-to-*cis* photoisomerization upon stimulation with a 365 nm LED, with a half-life of 0.37 min (Supplementary Fig. 25). When excited with an 850 nm LED with a ham layer, **AZO-EH** displayed *cis*-to-*trans* photoisomerization in the presence of air with a half-life of 1.28 min (Supplementary Fig. 26). The half-life of *cis*-to-*trans* isomerization, $t_{1/2\ cis\text{-}to\text{-}trans}$ = 82 min Supplementary Fig. 27), is slow compared to the solution without the ham layer

($t_{1/2\ cis\text{-}to\text{-}trans}$ = 1.28 min), which can be attributed to the excitation intensity-dependent nature of photoisomerization. Encouragingly, photoisomerization occurs even within an aqueous solution at physiological pH, suggesting potential applications of this technique to azobenzene-containing drugs.

The long half-life of triplet-sensitized *cis*-to-*trans* isomerization of **AZO-EH** in the micellar environment prompted the examination of the contribution of temperature. The *cis*-to-*trans* isomerization studies of **AZO-EH** in PF-127 micelles were carried out at biologically relevant temperatures (30, 35 and 40 °C), where the half-life ($t_{1/2\ cis\text{-}to\text{-}trans}$) was found to be 1589, 888 and 488 min, respectively (Supplementary Fig. 28). These results demonstrate minimal thermal contribution to *cis*-to-*trans* photoisomerization of **AZO-EH** during triplet-sensitization at physiological temperature, (Supplementary Fig. 27). The effect of photosensitizer concentration on the kinetics of isomerization was also measured by titrating the same concentration of **AZO-EH** (30 μM) against varying **ZnPc1** concentrations (0.5 μM to 10 μM) in PF-127 micelles in water (Supplementary Figs. 29 and 30). The results show that *cis*-to-*trans* isomerization could be achieved even at 0.5 μM concentration of **ZnPc1**. Moreover, the half-life ($t_{1/2\ cis\text{-}to\text{-}trans}$) decreased up to 5 μM concentration of **ZnPc1**, followed by stabilization thereafter (Supplementary Fig. 30).

The composition of the photostationary state (PSS) of **AZO-EH** in micellar solutions following triplet-sensitization was analyzed using ^{1}H NMR spectroscopy. The measurements were first conducted in $CDCl_3$ and PF-127-D_2O solution without photosensitizer (**ZnPc1**), serving as a reference standard (Supplementary Figs. 31–42, 43–52). In the $CDCl_3$ environment, irradiation at 365 nm for 2 min resulted in a maximum of 95% *cis*-**AZO-EH** in the PSS. Conversely, subsequent back-conversion through irradiation at 455 nm for one min reduced the *cis*-**AZO-EH** to 31% in the PSS (Supplementary Table 2). In the **AZO-EH**-PF-127-D_2O solution, a 5 min exposure to 365 nm light achieved 99% *cis*-**AZO-EH** in the PSS, both in the absence of (Table S3) and the presence of **ZnPc1** (Supplementary Figs. 53–57 and Table S4). Upon back-conversion with 455 (Supplementary Table 3) or 730 nm (Supplementary Figs. 58–62 and Supplementary Table 4) irradiation for 10 min, *cis*-**AZO-EH** decreased to 15%, and 18%, respectively, in the PSS. Therefore, the relative composition of *cis* and *trans*-**AZO-EH** in the PSS after back-conversion remains almost similar in micellar solution regardless of direct or indirect irradiation. The feasibility of triplet-sensitized *cis*-to-*trans* isomerization was also tested on the azobenzene-based drug molecule **PAI**[15,33] in phosphate buffer solution of PF-127 micelles at pH 7.4 (Fig. 5a, b).

PAI is an agonist of muscarinic acetylcholine receptor subtype 2 (M_2 mAChR)[15,33]. The M_2 mAChRs belong to the class A G-protein coupled receptors (GPCRs) and are primarily found in the heart. Stimulation of the M_2 mAChRs by the parasympathetic nervous system leads to a decrease in heart rate and an increase in atrioventricular conduction time. Previous studies have shown that **PAI** can act as a dualsteric drug, allowing for the photo-control of M_2 mAChR activity using one-photon (460 nm LED)[15], two-photon (840 nm pulsed laser)[15] and three-photon (1560 nm pulsed laser)[33] absorption techniques, albeit at high photon fluences. Here, **PAI** isomerization was controlled through photoactivation using triplet sensitization upon excitation with a 730 nm continuous wave LED at a significantly reduced excitation power density (46 mW cm^{-2}) compared to that of 2PA (Fig. 5c, d). The successful result in an aqueous, cellular-like environment within the phototherapeutic window prompted in vivo experiments to explore the application of triplet-sensitized photoswitching in photopharmacology.

In vivo Photomodulation of Cardiac function via TSP

The development of red-light photoswitchable drugs must satisfy challenging criteria of aqueous solubility, reversible switching behavior, and absence of immunogenicity[13]. Activation of photoswitchable drugs has been demonstrated by two-photon excitation at NIR wavelengths (800–900 nm)[30,63–65] and three-photon excitation at 1560 nm (mid-IR)[11], but the requirement for large laser and optical equipment confines the methods to research laboratories. Upconversion in optogenetics[5] and photo-pharmacology[66] has been achieved with continuous wave (CW) light sources (LED or lasers) at 980 nm, but requires injecting potentially toxic, heavy metal-laden nanoparticles. Optogenetic defibrillation, which utilizes red light to regulate arrhythmias in the heart of transgenic mice, is another emerging technique; however, it necessitates genetic mutation of the receptive cardiac tissue with light-sensitive channelrhodopsin-2 (ChR2)[6]. Optical defibrillation through the reversible photoswitching of azobenzene-labeled azobupivacaine 2 (AB2) represents another promising approach for the modulation of cardiac electrophysiology by reversibly inhibiting voltage-gated Na^+ and K^+ channels. Nonetheless, this technique relies on UV-blue light for the reversible photoswitching[67]. Developing synthetic biocompatible photosensitizers that allow photoactivation of drugs with CW IR light by simple triplet sensitization could have a wide impact in photo-pharmacology and phototherapies. Accordingly, the feasibility of controlling cardiac activity in vivo with 730 nm illumination via triplet-sensitized photoisomerization of the azobenzene-containing **PAI** was examined. **PAI** has been demonstrated to serve as a photoswitchable agonist capable of activating muscarinic M_2 receptors at picomolar potency with subtype selectivity[15]. The experiments were conducted on albino *Xenopus laevis* tadpoles, refs. S7–S11, which are translucent and allow non-invasive real-time visualization and quantification of cardiac activity and efficient photoswitching of drugs by CW light sources such as LEDs to dynamically control cardiac function (Fig. 6a–d) [6,15].

The drug **PAI** was dissolved in an aqueous micellar solution along with the triplet photosensitizer **ZnPc1** for testing (Fig. 1d). The micelles act as carriers to deliver both **PAI** and **ZnPc1** to the M_2 mAChR membrane receptor. Before the introduction of this formulation into a tadpole water, followed by 730 nm excitation, photoswitching experiments with UV-blue light were performed to demonstrate feasibility at normal absorption wavelengths. **PAI** reversibly photoisomerizes between the *trans* form (dark-relaxed and under blue 455 nm LED illumination) and *cis* form (under 365 nm UV illumination), displaying higher and lower pharmacological activity, respectively (Supplementary Fig. 63a–e).

Application of 30 μM *trans* **PAI** to water decreases the tadpole heartbeat, leading to cardiac arrest (Supplementary Fig. 63b), which can be reversed by UV illumination with a 365 nm LED (Supplementary Fig. 63c), as reported[15]. This effect is reversible due to **PAI** isomerization from *cis*-to-*trans* (Supplementary Fig. 63d). The results are quantified by the averaged amplitude of cardiac contraction (Supplementary Fig. 63e) and by the heartbeat frequency (Supplementary Fig. 64). After control experiments, here, an in vivo triplet-sensitized photoswitching assay of **PAI** combined with **ZnPc1** was implemented (Fig. 6e). First, a 3 min waiting period was recorded to test the stabilization and health status of the tadpoles. Then, the tadpole medium was replaced with an inactive, pre-irradiated 30 μM *cis*-**PAI** solution combined with or without 10 μM **ZnPc1** encapsulated by 2% PF127 in 0.1X MBS. This solution produced only minor changes in heartbeat (Fig. 6e). Following this, 730 nm LED illumination was applied in consecutive 10 min intervals to allow triplet sensitization of **PAI** for *cis*-to-*trans* isomerization while minimizing sample warming. Figure 6f shows that in the initial absence of PAI, the tadpole cardiac activity (amplitude of cardiac contraction and cardiac frequency, see Supplementary Fig. 65) remained stable and only changed slightly upon application of 30 μM *cis*-**PAI**. In contrast, cardiac activity was reduced during consecutive 10 min 730 nm LED illumination periods, while no significant effects were observed with illumination in the absence of **ZnPc1** or **PAI** (Fig. 6f). These controls rule out possibilities like **PAI** being activated thermally or cardiac activity being reduced by

https://doi.org/10.1038/s41467-025-61301-3

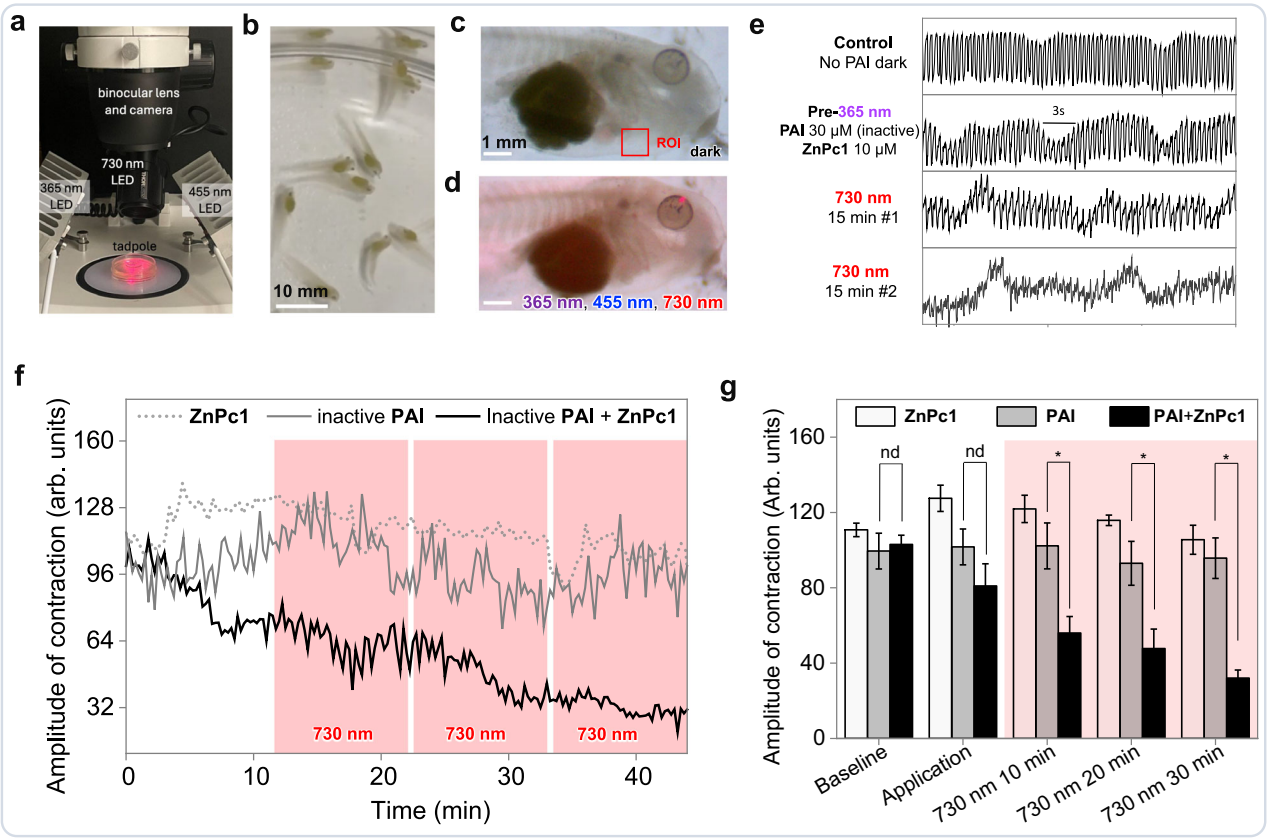

Fig. 6 | Modulation of cardiac activity mediated by triplet-sensitized photoswitching of muscarinic drug PAI in the phototherapeutic window. a Apparatus to optically record cardiac activity in frog tadpoles, including a binocular microscope equipped with a camera and LEDs with 365, 455, and 730 nm wavelengths. **b** Freely swimming tadpoles at stages 46–48. **c** Image representing the application of 0.23 mM pancuronium dibromide solution to immobilize the tadpole (stage 47) for long-term imaging of cardiac activity under dim light at 32 frames per second (fps) video recording. A region of interest (ROI) is placed at the edge of the heart to record the beating. **d** Image representing the setup for applying compounds to the medium and illuminating at wavelengths of interest (365, 455 and 730 nm LED in the photo). **e** Time course of the mean ROI intensity of heartbeat under the conditions indicated in the labels: control in the absence of **PAI** and light, inactive 365 nm-preilluminated (I_o = 10.9 mW cm^{-2}) 30 μM **PAI** together with 10 μM **ZnPc1** photosensitizer in the dark, and effect of illuminating the mix with 730 nm light (I_o = 42 mW cm^{-2}) in consecutive 15 min periods. **f** Time course of the amplitude of cardiac contraction during controls, compound application in the dark, and three consecutive 10 min periods of 730 nm illumination (shaded in red). The black line represents inactive 365 nm-preilluminated 30 μM **PAI** with 10 μM **ZnPc1**, and 2% PF127 in 0.1X MBS diluted buffer, the gray line shows the control experiment in the absence of the triplet photosensitizer **ZnPc1**, and the dotted line represents the control corresponding to the triplet sensitizer alone (10 μM **ZnPc1** and 2% PF127 in 0.1X MBS). The corresponding frequency plots are shown in the Supplementary Information. **g** Quantification of the experiments in panels (**e**, **f**). White bars represent the mean amplitude of contraction measured at intervals of 15 s during each experimental phase (baseline, application, 730 nm 10 min, 20 min, and 30 min) following treatment with the sensitizer (**ZnPc1**) alone (n = 3 animals, biological replicates). Gray bars represent measurements with **PAI** alone (n = 2 animals, biological replicates), and black bars represent the combination of **ZnPc1** and **PAI** (n = 3 animals, biological replicates). Each data point shown represents independent biological replicates derived from separate animals. Due to ethical considerations regarding animal use, the number of biological replicates was kept minimal. Error bars indicate the standard error of the mean (SEM). Statistical significance (*) indicates $p < 0.05$ when comparing the combination treatment (**PAI** + sensitizer) to sensitizer alone, multiple unpaired t test. "nd" indicates no significant difference.

ZnPc1-photoemitted species. The decrease in amplitude of cardiac contraction is quantified in Fig. 6g and is comparable to that observed with active *trans*-**PAI**, although changes are significantly slower, probably due to limited penetration of micelles in tissue and/or photoconversion in the experimental conditions. Future studies will be focused on testing different molecular weight Pluronics for enhanced tissue penetration and proximity of photoswitchable drugs to photosensitizers to accelerate overall triplet sensitization, in addition to designing covalently linked photosensitizer-photoswitch pairs. Overall, the results to date indicate that **PAI** can be converted from the inactive *cis* form to the active *trans* form in vivo by means of **ZnPc1**-mediated triplet sensitization under 730 nm illumination. Since the light sources and reagents are widely available, the triplet photosensitization method opens an alternative avenue to activate photoswitchable drugs using tissue-penetrating, non-invasive illumination.

Discussion

The field of photo-pharmacology aims to exploit the rich array of photochemical phenomena for non-invasive applications in the biomedical arena. Here, triplet-sensitized photoswitching has been examined as a means of utilizing light in the phototherapeutic window to exercise structural control of the azobenzene motif. A comprehensive experimental investigation conducted across various matrices such as a skin mimic and micelles has demonstrated that (1) the action spectrum of azobenzenes can be effectively shifted towards the NIR-I region (850 nm) by 400 nm, and (2) this red-shift could be achieved at an excitation power of only 2.62 mW cm^{-2}, after passing through animal tissue. The strategy is a viable alternative to 2PA, ESA, and TTA-UC for achieving biological photoactivation at very low levels of photon fluence within the phototherapeutic window. As one example, the heart rate of frog tadpoles is modulated through triplet-sensitized *cis*-to-*trans* photoisomerization of a dualsteric drug, Phthalimide-Azo-

Iperoxo (**PAI**), upon excitation of a photosensitizer, **ZnPc1**, with 730 nm LED light at an excitation power of 42 mW cm^{-2}. This excitation power level is substantially below the established tolerance limit of skin (200 mW cm^{-2}).

In summary, triplet-sensitized photoisomerization in biological environments presents an alternative approach to trigger photoswitchable drugs through non-invasive, tissue-penetrating illumination. As such, the demonstrated approach represents an important advance in the domain of photopharmacology. The colocalization of the photosensitizer and of the photoswitch is crucial for triplet-sensitization. We assume that the colocalization was accomplished here due to the presence of the orthosteric site of M_2 mAChR within the hydrophobic core of the membrane, which serves as an ideal environment for housing hydrophobic chromophores. However, while it is crucial to understand the mechanism by which chromophores encapsulated in PF-127 micelles are internalized, this would deserve a separate study about the colocalization of the dyes upon their delivery using micelles. Another key issue is the *trans*-to-*cis* photoisomerization with the UV light and singlet oxygen generation during the interaction of photosensitizer with the molecular oxygen in vivo. Future molecular designs are envisaged that extend beyond the present proof-of-principle experiments wherein the photosensitizer and photo-drug are linked together along with the singlet oxygen quencher, and the electronic structure of azobenzene is tailored to shift the action spectrum of *trans*-to-*cis* isomerization towards the red region. For example, recent work by Thorn-Seshold and co-workers (submitted in chemrxiv) demonstrated in vitro photocontrol of the SNAP-mGluR2 expression in granule cells of the dentate gyrus brain slices due to *cis*-to-*trans* photoisomerization of a bioactive azobenzene-photosensitizer dyad upon irradiation with 660 or 740 nm light[68]. Taken together, the foundation is solid for the next step: exploring such systems for efficient and broad-spectrum photocontrol of pharmacology in the phototherapeutic window.

Methods

The biological research carried out in this work complies with all relevant ethical regulations set by the ethical commission of the University of Barcelona.

Preparation procedure of G-TXr-AZO-N-PdNc1, G-TXr-AZO-MM-PdNc1, and G-TXr-AZO-EH-PdNc1 biomimetic films

Films were prepared using the following procedure. A solution composed of 12 μL of **AZO-N**, or **AZO-MM** or **AZO-EH** (40 mM in toluene) and 70 μL of **PdNc1** (716 μM in toluene) was concentrated under a N_2 atmosphere in a glass vial. The residual mixture was treated with 0.026 g of TXr and stirred at 60 °C for complete solubilization of chromophores. The resulting solution was treated with 1 mL of Millipore grade water followed by stirring. The aqueous solution of chromophores and TXr was treated with 0.22 g of gelatin type A (G), followed by stirring at 70 °C for 10 min. The hot solution was allowed to rest at room temperature for 2 min, followed by drop-casting of 260 μl of the solution on a 3 × 1 cm glass plate and air drying for 24 h. The resulting air-dried films contained the following constituents: TXr = 10.5%, gelatin = 89.4%, **PdNc1** = 203 μmol $kg^{-1}$and AZO compounds (**AZO-N, AZO-MM** and **AZO-EH** = 1.95 mmol kg^{-1}. The faint yellow semi-transparent film obtained after air drying for 24 h was used for the photoisomerization measurements upon excitation with 340, 365 and 850 nm LEDs.

Preparation of the G-TXr-AZO-EH-BC1 biomimetic film

A solution composed of 12 μL of **AZO-EH** (40 mM) and 100 μL of **BC1** (500 μM) in toluene was concentrated under N_2 atmosphere in a glass vial. To the residual mixture added 0.026 g of TXr and stirred at 60 °C until the chromophores were fully dissolved. To the resulting solution added added 1 mL of Millipore grade water, followed by stirring. Into the aqueous solution of chromophores added 0.22 g of gelatin type A (G), followed by stirring at 70 °C for 10 min. The hot solution was allowed to rest at room temperature for 2 min, followed by drop-casting of 260 μl of the solution on a 3 × 1 cm glass plate and air drying for 24 h. The air-dried films contain TXr = 10.5%, gelatin = 89.4%, **BC1** = 203 μmol.kg-1and **AZO-EH** = 1.95 mmol kg^{-1}.

Preparation of the G-TXr-AZO-EH-ZnPc1 biomimetic film

A solution composed of 12 μL of **AZO-EH** (40 mM) and 157 μL of **ZnPc1** (317.5 μM) in toluene was concentrated under a N_2 atmosphere in a glass vial. The residual mixture was treated with 0.026 g of TXr and stirred at 60 °C until the chromophores were fully dissolved. The resulting solution was treated with 1 mL of Millipore grade water followed by stirring. The aqueous solution of chromophores was treated with 0.22 g of gelatin type A (G), followed by stirring at 70 °C for 10 min. The hot solution was allowed to rest at room temperature for 2 min, followed by drop-casting of the 260 μl of the solution on a 3 × 1 cm glass plate and air drying for 24 h. The resulting air-dried films contained TXr = 10.5%, gelatin = 89.4%, **BC1** = 203 μmol kg^{-1} and **AZO-EH** = 1.95 mmol kg^{-1}.

Preparation of PF-127-AZO-EH-ZnPc1 micelles solutions

A solution composed of 12 μL of **AZO-EH** (40 mM), 50 μL of **ZnPc1** (317.5 μM) and 0.02 g of PF-127 in toluene was concentrated under a N_2 atmosphere in a glass vial. The residual mixture was treated with 1 mL of Millipore grade H_2O, followed by stirring in an ice bath to dissolve PF-127. The resulting solution was brought to room temperature. The resulting micellar solution contained the following constituents: **AZO-EH** = 0.48 mmol L^{-1}, **ZnPc1** = 15.85 μmol L^{-1} and PF-127 = 2%. This stock solution was diluted 20x with 2% PF-127 in water. Photoswitching measurements were carried out in a 0.1 cm pathlength quartz cuvette with the following concentrations, **AZO-EH** = 24 μmol L^{-1}, **ZnPc1** = 0.8 μmol L^{-1} and PF-127 = 2%. Temperature dependent experiments were carried out in 1 cm pathlength quartz cuvette. For this 185 μL of **AZO-EH**-PF-127 aqueous solution (480 μM) is added to 2.315 mL of PF-127 (2%) aqueous micellar solution to keep the absorbance below 1.0. Final **AZO-EH** concentration = 35.5 μM. The samples for UV-Vis titrations of **AZO-EH** (30 μM) against different concentrations of **ZnPc1** (0.5, 2.5, 5, and 10 μM) were prepared by mixing 62.5 μL of **AZO-EH** (480 μM in 2% PF-127 in water) with 10, 50, 100, and 200 μL of **ZnPc1** (50 μM in 2% PF-127 in water), and 927.5, 887.5, 837.5 and 737.5 μL of 2% PF-127 in water respectively.

Preparation of AZO-EH $CDCl_3$ solution and ^{1}H NMR characterization to measure composition of AZO-EH photostationary state in $CDCl_3$ as reference

A 5 mM solution of **AZO-EH** was prepared by dissolving 1.55 mg of **AZO-EH** in $CDCl_3$. The solution was irradiated with 365 nm LED, for 15, 30, 60, 120, 180 and 240 s. ^{1}H NMR spectra were recorded (Supplementary Figs. 31–36). The relevant peaks of the **AZO-EH** between 8.5-6 ppm, 4.5-3.5 ppm, and 2-0.5 ppm undergo shifts and a decrease/increase in intensity. The conversion could also be observed by a change in the color of the solution from yellow to orange (Supplementary Fig. 31). The peaks were identified to originate from the **AZO-EH** by comparison to the solution without the **AZO-EH** present. The sample solution was irradiated in a second irradiation experiment with 455 nm for 15, 30, 60, 150, 300 s for back-conversion. ^{1}H NMR spectra were recorded, and the changes were seen to be reversible (Supplementary Figs. 37–42) The color change is also reversible (Supplementary Fig. 37). The composition of the photostationary state was determined for both irradiation experiments by integrating the changes in relevant peak areas and is provided in Supplementary Table 2.

Preparation of PF-127-AZO-EH-D_2O micelles solution for ^1H NMR characterization to measure the composition of the photostationary state

A 5 mM solution of **AZO-EH** in D_2O was prepared by mixing 1.55 mg of **AZO-EH** with 0.02 g via heating at 70 °C for 5 min, followed by the addition of 1000 μL of D_2O and stirring in the ice bath for 10 min for complete solubilization of all components. As a reference experiment, the **AZO-EH** (5 mM)-PF127 (2%)-D_2O solution was irradiated with 365 and 455 nm, for 15, 30, 60, 120, 180 and 240 s, followed by recording of their ^1H NMR spectra after each irradiation. First, the sample was irradiated with 365 nm LED, and ^1H NMR spectra were recorded (Supplementary Figs. 43–47). The relevant peaks of the **AZO-EH** between 6-8 ppm, and 0.75-0.4 ppm undergo shifts and a decrease/increase in intensity. The conversion could also be observed by a color change of the solution from yellow to orange (Supplementary Fig. 43). The peaks were identified to originate from the **AZO-EH** by comparison to the solution without the **AZO-EH** present. The sample solution was irradiated in a second irradiation experiment with 455 nm for 15, 30, 60, 150, 300 s for back-conversion. ^1H NMR spectra were recorded, and the changes were seen to be reversible (Supplementary Figs. 48–52). The color change is also reversible (Supplementary Fig. 48). The composition of the photostationary state was determined for both irradiation experiments by integrating the changes in relevant peak areas and is provided in Supplementary Table 3.

Preparation of PF-127-AZO-EH-ZnPc1-D_2O micellar solution for ^1H NMR characterization to measure the composition of the photostationary state

A 5 mM solution of **AZO-EH** doped with 50 μM of **ZnPc1** in D_2O was prepared by mixing 1.55 mg of **AZO-EH** with 0.02 g of PF-127, via heating at 70 °C for 5 min, followed by the addition of 784 μL of D_2O, and 216 μL of **ZnPc1**-PF-127 (2%)-D_2O solution (231 μM). The solution was stirred in an ice bath for 10 min for complete solubilization of all components. First, the NMR sample was irradiated with 365 nm LED, for a total of 5 min. ^1H NMR spectra were recorded (Supplementary Figs. 53–57). The relevant peaks of the **AZO-EH** between 6-8 ppm, and 0.75-0.4 ppm undergo shifts and a decrease/increase in intensity. The conversion could also be observed by a change in the color of the solution from yellow to orange (Supplementary Fig. 53). The peaks were identified to originate from the **AZO-EH** by comparison to the solution without the **AZO-EH** present. When irradiated in a second irradiation experiment with 730 nm for in total of 10 min, while a ^1H NMR spectrum was recorded after various time steps, and the changes were seen to be reversible (Supplementary Figs. 58–62). The color change is also reversible (Supplementary Fig. 58).

Preparation of PF-127-PAI-ZnPc1 micelles solution

2.5 μL of **ZnPc1** (317.5 μM in toluene) and 0.005 g of PF-127 dissolved in toluene were evaporated under N_2 atmosphere in a glass vial. The residual mixture was treated with 250 μL of **PAI** solution in phosphate buffer pH. 7.4, followed by stirring in an ice bath to dissolve PF-127. The resulting solution was brought to room temperature for the photoswitching measurements in a 0.1 cm pathlength quartz cuvette. The final measurement concentrations were as follows: **AZO-EH** = 50 μmol L^{-1}, **ZnPc1** = 3 μmol L^{-1} and PF-127 = 2%.

Animal housing

Albino Xenopus laevis (Nasco Ltd) ref. S7 embryos were obtained by natural mating and sustained until 3-4 days post-fertilization (dpf) in 0.1X Marc's modified Ringer's (MMR) solution within a dark incubator set at 24 °C. Subsequently, the tadpoles were relocated to tanks containing Xenopus water, prepared by dissolving 8 g of Instant Ocean salt (Instant Ocean) in 20 L of distilled water. Tadpoles were maintained at a density of 20–30 animals per litre, at a constant temperature of 24 °C, and were fed spirulina daily. All procedures adhered to the ethical standards set by the ethical commission of the University of Barcelona. Xenopus tropicalis tadpoles, corresponding to developmental stages 44–48 according to Nieuwkoop and Faber ref. S8 were immobilized in 0.23 mM Pancuronium dibromide solution (PCD) (Merck, Cat no. P1918) for 10 min due to its higher cardiac tolerance and non-UV dependent effects ref. S10 before being transferred to a custom chamber containing 150 μL of 0.1x Modified Barth's Saline (MBS) prepared by 10x stock containing 800 mM NaCl, 10 mM KCl, 10 mM $MgSO_4{\cdot}7H_2O$, 50 mM HEPES free acid, 25 mM $NaHCO_3$; adjust the pH to 7.8 with NaOH and diluted in milli-Q water ref. S11.

Characterization techniques

Scanning electron microscopy. The cross-section scanning electron microscopy (SEM) images of the **G-TXr-AZO-EH** film were obtained using JEOL JSM-7800F Prime FEG SEM. The acceleration voltage is set to 10 kV, and a secondary electron detector is used. Before SEM observation, the sample is dried under vacuum for two days and coated with gold using the Edwards S150B gold sputter. The cross-section is obtained by breaking the film in half with hands.

X-ray diffraction measurements. X-ray diffractograms of the **G-TXr-AZO-EH** film is measured using Bruker the D8 DISCOVER is an X-ray diffraction instrument equipped with four motorized axes stage, having as typical applications: XR Reflectometry, Rocking measurements, RSM measurements and structural phase identification.

UV-Vis spectroscopy measurements. UV-Vis measurements of the chromophores solution and solid sample is done using a UV-Vis-NIR spectrophotometer Jasco V-770 with operational range of 190–3300 nm and FLS980 (Edinburgh Instruments). Samples were excited with at 365, 340, 455, 730, and 850 nm LED Thorlabs integrated with collimator and 340 nm UV-lamp, and 850 nm laser. LED emission power is measured with a standard Photodiode Power Sensor, ThorLabs S120VC. Solution state spectra were recorded in a quartz cuvette of 1 cm to 0.1 cm path length.

Fluorescence measurements. The steady-state FL emission spectra were measured using a back-thinned CCD spectrometer PMA-12 (Hamamatsu). Phosphorescence was measured with a time-gated iCCD camera, New iStar DH340T (Andor), after exciting the samples with the emission of a tunable-wavelength optical amplifier (Ekspla) pumped by a nanosecond Nd^{3+}:YAG laser (wavelength – 850 nm, pulse duration – 5 ns, repetition rate – 1 kHz).

^1H NMR measurements. The ^1H NMR spectra were recorded using a Bruker NMR Ascend 400 of 400 MHz equipped with two probes for a liquid and solid samples.

Cardiac activity measurements. Video recordings of tadpole hearts were conducted using a microscope equipped with an OptixCam Summit Series OCS-D3K2-5 camera that can capture more than 30 frames per second to resolve the ~1 Hz tadpole heartbeats. The recordings were acquired using ToupLite software, which enhances visual contrast to improve cardiac imaging, and the video streams were converted to the AVI format12 recordings were briefly paused during compound addition and changes in illumination conditions. Video information and data analysis were extracted and executed with custom scripts based on ImageJ13 for AVI file analysis and subsequently converted to csv format for further analysis ref. S12.

The illumination protocol established for control and treatment video recordings followed the procedure described below. LED irradiance values were measured by a Thorlabs PM101/PD TH optical power meter equipped with a Thorlabs S120VC sensor with a diameter of 9.5 mm. A three-minute dim light period (0.26 mW cm^{-2}) is allocated solely for imaging to establish baseline activity, followed by a 10 min

incubation of 30 µM **PAI** (with or without 10 µM **ZnPc1**, encapsulated in 2 % PF127 in 0.1X MBS) pre-irradiated under UV (365 nm 11 mW cm^{-2}) for 5 min to allow for enough trans-to-cis isomerization. Subsequently, 10 min 730 nm illumination (42 mW cm^{-2}) with a Thorlabs M730L5 LED is applied for three cycles to achieve *trans*-to-*cis* isomerization, with 2-min intervals of waiting period under dim light between each cycle.

Tadpoles ($n = 6$) were initially paralyzed with PCD as described earlier, placed in MBS, and video recorded under the established illumination protocol in the absence of **PAI** and **ZnPc1** combination to assess the effect of light alone on cardiac activity and to verify control conditions. Subsequently, each tadpole is exposed to a 30 µM **PAI** with 10 µM **ZnPc1** ($n = 3$) and without **ZnPc1** ($n = 3$) in MBS with 2% PF127 micelles and is subjected to the same illumination protocol to observe the light-dependent effects of the drug alone. One additional animal is tested to evaluate the effect of 10 µM **ZnPc1** alone in MBS with 2% PF127 without illumination cycles.

Quantification of the experiments in panels (f, g) in Fig. 6 main manuscript is performed by calculating the amplitude and frequency of cardiac contraction as a function of time and illumination in the presence and in the absence of **ZnPc1** (black and white bars, respectively). The results were obtained in 5 different animals ($n = 2$ control tadpoles without **ZnPc1**, $n = 3$ tadpoles treated with **ZnPc1**) and analyzed statistically using unpaired *t* tests with data from experiments with inactive **PAI** + **ZnPc1** versus inactive **PAI** without **ZnPc1** as the main factors, along with baseline measurements, compound application, and consecutive 730 nm illumination cycles as their interactions.

Data analysis and statistics

The videos capturing cardiac movement were processed to generate sinusoidal signals representing the grayscale intensity distribution within a selected region of interest (ROI) Fig. 6c (manuscript). This allowed recording tadpole cardiac movements and quantification of contraction amplitude and frequency over time (Fig. 6d, e and Supplementary Figs. 63 and 64). The amplitude of contraction data is extracted from the signal peaks occurring in 15 s intervals, after filtering out excessive noise to identify actual beating events. This involved identifying maximum peaks with high standard deviation within adjacent peaks, the range of which is determined empirically by examining the baseline dataset for each experiment. In addition, cardiac frequency is calculated based on the number of real beating events observed within every 15 s. Both the time course of cardiac parameters (amplitude of contraction and cardiac frequency) is plotted as a function of time (Fig. 6f, g and Supplementary Fig. 65).

Statistical analyses were conducted using an unpaired *t* test, incorporating data from experiments involving inactive **PAI** + **ZnPc1** and inactive **PAI** without **ZnPc1** as main factors, along with baseline measurements, compound applications, and 730 nm illumination cycles as their interactions ref. S13.

Reporting summary

Further information on research design is available in the Nature Portfolio Reporting Summary linked to this article.

Data availability

All data that support the findings of this study are presented in the manuscript and Supplementary Information, or are available from the corresponding author upon request. Source data are also provided in this paper.

References

1. Liu, Q., Feng, W., Yang, T., Yi, T. & Li, F. Upconversion luminescence imaging of cells and small animals. *Nat. Protoc.* **8**, 2033–2044 (2013).
2. Jewell, M. P., Greer, M. D., Dailey, A. L. & Cash, K. J. Triplet-triplet annihilation upconversion based nanosensors for fluorescence detection of potassium. *ACS Sens.* **5**, 474–480 (2020).
3. Wang, Y. & Kohane, D. S. External triggering and triggered targeting strategies for drug delivery. *Nat. Rev. Mater.* **2**, 17020 (2017).
4. Yang, D. et al. Current advances in lanthanide ion (Ln^{3+})-based upconversion nanomaterials for drug delivery. *Chem. Soc. Rev.* **44**, 1416–1448 (2015).
5. Chen, S. et al. Near-infrared deep brain stimulation via upconversion nanoparticle–mediated optogenetics. *Science* **359**, 679–684 (2018).
6. Bruegmann, t et al. Optogenetic defibrillation terminates ventricular arrhythmia in mouse hearts and human simulations. *J. Clin. Invest.* **126**, 3894–3904 (2016).
7. Crocini, C. et al. Optogenetics design of mechanistically based stimulation patterns for cardiac defibrillation. *Sci. Rep.* **35628**, 1–7 (2016).
8. Swamy, P. C. A. et al. Near Infrared (NIR) absorbing dyes as promising photosensitizer for photo dynamic therapy. *Coord. Chem. Rev.* **411**, 213233 (2020).
9. Lo, P.-C. et al. The unique features and promises of phthalocyanines as advanced photosensitisers for photodynamic therapy of cancer. *Chem. Soc. Rev.* **49**, 1041–1056 (2020).
10. Dąbrowski, J. M. et al. Engineering of relevant photodynamic processes through structural modifications of metallotetrapyrrolic photosensitizers. *Coord. Chem. Rev.* **325**, 67–101 (2016).
11. Vickerman, B. M., Zywot, E. M., Tarrant, T. K. & Lawrence, D. S. Taking phototherapeutics from concept to clinical launch. *Nat. Rev. Chem.* **5**, 816–834 (2021).
12. Klán, P. et al. Photoremovable protecting groups in chemistry and biology: reaction mechanisms and efficacy. *Chem. Rev.* **113**, 119–191 (2013).
13. Castagna, R., Maleeva, G., Pirovano, D., Matera, C. & Gorostiza, P. Donor–acceptor stenhouse adduct displaying reversible photoswitching in water and neuronal activity. *J. Am. Chem. Soc.* **144**, 15595–15602 (2022).
14. Samanta, S. et al. Photoswitching azo compounds in vivo with red light. *J. Am. Chem. Soc.* **135**, 9777–9784 (2013).
15. Riefolo, F. et al. Optical control of cardiac function with a photoswitchable muscarinic agonist. *J. Am. Chem. Soc.* **141**, 7628–7636 (2019).
16. Garrido-Charles, A. et al. Fast photoswitchable molecular prosthetics control neuronal activity in the cochlea. *J. Am. Chem. Soc.* **144**, 9229–9239 (2022).
17. Boyer, J.-C., Carling, C.-J., Gates, B. D. & Branda, N. R. Two-way photoswitching using one type of near-infrared light, upconverting nanoparticles, and changing only the light intensity. *J. Am. Chem. Soc.* **132**, 15766–15772 (2010).
18. Beharry, A. A. & Woolley, G. A. Azobenzene photoswitches for biomolecules. *Chem. Soc. Rev.* **40**, 4422–4437 (2011).
19. Vepřek, N. A. et al. Optical control of G-Actin with a photoswitchable latrunculin. *J. Am. Chem. Soc.* **146**, 8895–8903 (2024).
20. Dolai, A. et al. Photoisomerization and light-controlled antibacterial activity of fluoroquinolone-azoisoxazole hybrids. *ChemBioChem***25**, e202300851 (2024).
21. Xiao, D. et al. Azobenzene-based linker strategy for selective activation of antibody–drug conjugates. *Angew. Chem. Int. Ed.* **63**, e202310318 (2024).
22. Volarić, J. et al. Visible light control over the cytolytic activity of a toxic pore-forming protein. *ACS Chem. Biol.* **19**, 451–461 (2024).
23. Griffiths, J. Photochemistry of azobenzene and its derivatives. *Chem. Soc. Rev.* **1**, 481–493 (1972).
24. Dong, M. et al. Near Infrared photoswitching of azobenzenes under physiological conditions. *J. Am. Chem. Soc.* **139**, 13483–13486 (2017).
25. Dong, M., Babalhavaeji, A., Samanta, S., Beharry, A. A. & Woolley, G. A. Red-shifting azobenzene photoswitches for in vivo use. *Acc. Chem. Res.* **48**, 2662–2670 (2015).

26. Mandl, G. A., Rojas-Guterrez, P. A. & Capobianco, J. A. A NIR-responsive azobenzene-based supramolecular hydrogel using upconverting nanoparticles. *Chem. Commun.* **54**, 5847–5850 (2018).
27. Wu, W. et al. NIR-light-induced deformation of cross-linked liquid-crystal polymers using upconversion nanophosphors. *J. Am. Chem. Soc.* **133**, 15810–15813 (2011).
28. Jiang, Z., Xu, M., Li, F. & Yu, Y. Red-light-controllable liquid-crystal soft actuators via low-power excited upconversion based on triplet–triplet annihilation. *J. Am. Chem. Soc.* **135**, 16446–16453 (2013).
29. Cabré, G. et al. Rationally designed azobenzene photoswitches for efficient two-photon neuronal excitation. *Nat. Commun.* **10**, 907 (2019).
30. Izquierdo-Serra, M. et al. Two-photon neuronal and astrocytic stimulation with azobenzene-based photoswitches. *J. Am. Chem. Soc.* **136**, 8693–8701 (2014).
31. Jerca, F. A., Jerca, V. V. & Hoogenboom, R. Advances and opportunities in the exciting world of azobenzenes. *Nat. Rev. Chem.* **6**, 51–69 (2022).
32. Ye, C., Zhou, L., Wang, X. & Liang, Z. Photon upconversion: from two-photon absorption (TPA) to triplet–triplet annihilation (TTA). *Phys. Chem. Chem. Phys.* **18**, 10818–10835 (2016).
33. Sortino, R. et al. Three-Photon Infrared Stimulation of Endogenous Neuroreceptors in vivo. *Angew. Chem. Int. Ed. Engl.* **62**, e202311181 (2023).
34. Zhou, B., Shi, B., Jin, D. & Liu, X. Controlling upconversion nanocrystals for emerging applications. *Nat. Nanotechnol.* **10**, 924–936 (2015).
35. Yang, Y. et al. Switching the NIR upconversion of nanoparticles for the orthogonal activation of photoacoustic imaging and phototherapy. *Nat. Commun.* **13**, 3149 (2022).
36. Sanders, S. N. et al. Triplet fusion upconversion nanocapsules for volumetric 3D printing. *Nature* **604**, 474–478 (2022).
37. Bharmoria, P., Bildirir, H. & Moth-Poulsen, K. Triplet-triplet annihilation based near infrared to visible molecular photon upconversion. *Chem. Soc. Rev.* **49**, 6529–6554 (2020).
38. Alachouzos, G., Schulte, A. M., Mondal, A., Szymanski, W. & Feringa, B. L. Computational design, synthesis, and photochemistry of Cy7-PPG, an efficient NIR-activated photolabile protecting group for therapeutic applications. *Angew. Chem. Int. Ed. Engl.* **61**, e202201308 (2022).
39. Gemen, J. et al. Disequilibrating azobenzenes by visible-light sensitization under confinement. *Science* **381**, 1357–1363 (2023).
40. Isokuortti, J. et al. Expanding excitation wavelengths for azobenzene photoswitching into the near-infrared range via endothermic triplet energy transfer. *Chem. Sci.* **12**, 7504–7509 (2021).
41. Bharmoria, P. et al. Far-red triplet sensitized *Z*-to-*E* photoswitching of azobenzene in bioplastics. *Chem. Sci.* **13**, 11904–11911 (2022).
42. Isokuortti, J. et al. Triplet sensitization enables bidirectional isomerization of diazocine with 130 nm redshift in excitation wavelengths. *Chem. Sci.* **14**, 9161–9166 (2023).
43. Monti, S., Gardini, E., Bortolus, P. & Amouyal, E. The triplet state of azobenzene. *Chem. Phys. Lett.* **77**, 115–119 (1981).
44. Bandara, H. M. D. & Burdette, S. C. Photoisomerization in different classes of azobenzene. *Chem. Soc. Rev.* **41**, 1809–1825 (2012).
45. Pitruzzello, G. Seeing into deep tissue. *Nat. Photon.* **17**, 376–377 (2023).
46. Tobin, D. J. Biochemistry of human skin-our brain on the outside. *Chem. Soc. Rev.* **35**, 52–67 (2006).
47. Masutani, K., Morikawa, M. -a & Kimizuka, N. A liquid azobenzene derivative as a solvent-free solar thermal fuel. *Chem. Commun.* **50**, 15803–15806 (2014).
48. Pucelik, B., Sułek, A. & Dąbrowski, J. M. Bacteriochlorins and their metal complexes as NIR-absorbing photosensitizers: properties, mechanisms, and applications. *Coord. Chem. Rev.* **416**, 213340 (2020).
49. Tran, V.-P. et al. Bacteriochlorin Syntheses – Status, Problems, and Exploration. *J. Porphyr. Phthalocyanines* **27**, 1502–1551 (2020).
50. Vairaprakash, P. et al. Extending the short and long wavelength limits of bacteriochlorin near-infrared absorption via dioxo- and bisimide-functionalization. *J. Phys. Chem. B* **119**, 4382–4395 (2015).
51. Takiff, L. & Boxer, S. G. Phosphorescence spectra of bacteriochlorophylls. *J. Am. Chem. Soc.* **110**, 4425–4426 (1988).
52. Topal, S. Z. et al. Modulation of the electronic and spectroscopic properties of Zn(II) phthalocyanines by their substitution pattern. *Dalton Trans.* **43**, 6897–6908 (2014).
53. Tobolskv, A. V. Cross-linking of gelatine by dehydration. *Nature* **215**, 509–510 (1967).
54. Farcet, J.-B., Kindermann, J., Karbiener, M. & Kreil, T. R. Development of a Triton X-100 replacement for effective virus inactivation in biotechnology processes. *Eng. Rep.* **1**, e12078 (2019).
55. Bharmoria, P. et al. Recyclable optical bioplastics platform for solid state red light harvesting via triplet–triplet annihilation photon upconversion. *J. Mater. Chem. A* **10**, 21279–21290 (2022).
56. Holmes, D. F., Lu, Y., Starborg, T. & Kadler, K. E. Collagen fibril assembly and function. *Curr. Top. Dev. Biol.* **130**, 107–142 (2018).
57. Isokuortti, J. et al. Endothermic and exothermic energy transfer made equally efficient for triplet–triplet annihilation upconversion. *J. Phys. Chem. Lett.* **11**, 318–324 (2020).
58. Goulet-Hanssens, A. et al. Electrocatalytic *Z* → *E* isomerization of azobenzenes. *J. Am. Chem. Soc.* **139**, 335–341 (2017).
59. Sandros, K. & Bäckström, H. L. J. Transfer of Triplet-state energies in the fluid solutions. *Acta Chem. Scand.* **16**, 958–968 (1962).
60. Sandros, K. Transfer of triplet-state energies in the fluid solutions. III reversible energy transfer. *Acta Chem. Scand.* **16**, 2355–2374 (1964).
61. Smith, M. H. Safe delivery of optical power from space. *Opt. Express* **8**, 537–546 (2001).
62. Akash, M. S. H. & Rehman, K. Recent progress in biomedical applications of Pluronic (PF127): Pharmaceutical perspectives. *J. Control Release* **209**, 120–138 (2015).
63. Carroll, E. C. et al. Two-photon brightness of azobenzene photoswitches designed for glutamate receptor optogenetics. *PNAS* **112**, E776–E785 (2015).
64. Pittolo, S. et al. Reversible silencing of endogenous receptors in intact brain tissue using 2-photon pharmacology. *PNAS* **116**, 13680–13689 (2019).
65. Kellner, S. & Berlin, S. Two-photon excitation of azobenzene photoswitches for synthetic optogenetics. *Appl. Sci.* **10**, 805 (2020).
66. Zhao, J. & Ellis-Davies, G. C. Intracellular photoswitchable neuropharmacology driven by luminescence from upconverting nanoparticles. *Chem. Commun.* **56**, 9445–9448 (2020).
67. Fehrentz, T. et al. Optical control of cardiac electrophysiology by thephotochromic ligand azobupivacaine 2. *Br. J. Pharm.* **182**, 1125–1142 (2025).
68. Baumgartner, B. et al. A general method for near-infrared photoswitching in biology, demonstrated by the >700 nm photocontrol of GPCR activity in brain slices. Preprint at https://doi.org/10.26434/chemrxiv-2024-vm4n3 (2024).

Acknowledgements

This work is developed within the scope of the La-Caixa junior research leadership-post doctoral project PHOLCEB (ID: 100010434, fellowship code: LCF/BQ/P122/11910023). P.B. and M.M. acknowledge La-Caixa foundation, the State Investigation Agency, through the Severo Ochoa Program for Centers of Excellence in R&D (CEX2023-001263-S) and project PID2021-123873NB-I00 for financial support. K.M.P. acknowledges funding from the European Research Council (No. 101002131), the Swedish Energy Agency, the Göran Gustafsson Foundation, the Swedish

Research Council, Swedish Research Council Formas, the European Research Council (ERC) under grant agreement CoG, PHOTHERM –101002131, the Catalan Institute of Advanced Studies (ICREA) and the European Union's Horizon 2020 Framework Program under grant agreement no. 951801. L.N. acknowledges the Erasmus + Traineeship Program. M.D., J.L., and K.K. acknowledge the "Universities' Excellence Initiative" program by the Ministry of Education, Science and Sports of the Republic of Lithuania under the agreement with the Research Council of Lithuania (project No. S-A-UEI-23-6). P.G. acknowledges EU Horizon 2020 Framework Program for Research and Innovation, including the European Innovation Council Pathfinder Open (Phototheraport, 101130883), Human Brain Project (WaveScalES, SGA3, 945539), and Information and Communication Technologies (Deeper, ICT-36-2020- 101016787). It is also supported by the Government of Catalonia (CERCA Program; AGAUR 2021-SGR-01410) and by the Spanish Ministry of Science and Innovation (DEEP RED, grant PID2019-111493RB-I00; EPILLUM, grant AEI/10.13039/501100011033; Research Network in Biomedicine eBrains-Spain, RED2022-134823-E). J.S.L. acknowledges support from the U.S. Department of Energy, Office of Science, Office of Basic Energy Sciences, Chemical Sciences, Geosciences and Biosciences Division, under Award Number DE-FG0205ER15661. Galyna Malieieva, Núria Camarero (Institute for Bioengineering of Catalonia), and Javier Palacios Sánchez (Parc Científic de Barcelona) are acknowledged for help with Xenopus ethical procedures, mating and manipulation, which were authorized by the Barcelona Biomedical Research Park (PRBB) Animal Research Ethics Committee and the Catalan Government (code #9891), and by Parc Científic de Barcelona (CEEA-PCB 21-036). Nuria Aliaga-Alcalde and Daniel Herrera Miranda are acknowledged for performing electrocatalytic measurements.

Author contributions

P.B., L.N., K.M.P., and P.G. conceptualized the idea of this work. L.N., P.B., and M.M. carried out the photoswitching studies in different materials. M.D., J.L., E.R., and K.K. carried out photoluminescence emission and quenching studies. P.G. group (E.O., P.B., V.C.M., F.R., C.M.) synthesized **PAI** and carried out in vivo studies in frog tadpoles. H.H. synthesized **AZO-MM** and carried out photoswitching studies using NMR spectroscopy, M.-a-M. and N.K. synthesized **AZO-EH**, K.H. and F.D. synthesized **ZnPc1**, and M.T. and J.S.L. synthesized **BC1**. P.B., K.M.P., E.O., and P.G. contributed to writing the first draft of the manuscript. M.T., J.S.L. and F.D. edited the first draft of the manuscript. All authors contributed to revise the final draft of the manuscript.

Competing interests

The authors declare no competing interests.

Additional information

Supplementary information The online version contains supplementary material available at https://doi.org/10.1038/s41467-025-61301-3.

Correspondence and requests for materials should be addressed to Pankaj Bharmoria, Pau Gorostiza or Kasper Moth-Poulsen.

Peer review information *Nature Communications* thanks the anonymous reviewers for their contribution to the peer review of this work. A peer review file is available.